 

PACS numbers: 42.55.Lt; 42.60.Lh
DOI: 10.1070/QE2003v033n10ABEH002514

# Theoretical model of a radio-frequency-discharge-pumped CO laser

I.V. Kochetov, A.P. Napartovich, S.A. Starostin

*Abstract*. **The theoretical model of a radio-frequency-discharge-pumped CO laser is described. The model consists of a block for calculating the spatial characteristics of a capacitive radio-frequency discharge along the interelectrode distance and the distribution of the translational temperature of the gas. Another block contains the equations of the vibrational kinetics and the condition for stationary lasing in the resonator. The model was used to calculate the energy and spectral parameters of the CO laser in the stationary regime for different temperatures of the walls and two different spatial intensity distributions. The results are compared with the experimental data reported in the literature.**

***Keywords***: *CO laser, slab laser, radio-frequency discharge.*

## 1. Introduction

Recently considerable progress has been achieved in the development of capillary and slab $CO_2$ and CO lasers excited by a capacitive transverse radio-frequency (RF) discharge (the frequency range 1 – 100 MHz). A gas mixture in these lasers is cooled with the help of electrodes to which the exciting radio-frequency voltage is applied (see, for example, Refs [1 – 3]). The RF discharge has a number of advantages over the direct current (DC) discharge. These are first of all a lower voltage of power supplies, the greater energy efficiency, a simple modulation, and the possibility to control the output power of lasers. The RF discharge is capable of exciting sufficiently large volumes of an active medium (in the case of planar geometry) without using external ionisation sources and proves to be more stable than the DC discharge. The matter is that, to provide current through the discharge gap in the RF discharge, it is not necessary to form a cathode layer to ensure the current closure to the electrode. In the RF discharge, a cathode and an anode are interchanged depending on the field phase, and the current closure near the electrode, which plays the role of the cathode at a given instant, provides the bias current.

**I.V. Kochetov, A.P. Napartovich** State Scientific Center of the Russian Federation, Troitsk Institute for Innovation and Fusion Research, 142190 Troitsk, Moscow region, Russia; e-mail: apn@triniti.ru
**S.A. Starostin** Univesity of Twente, 7500 AE Enschede, The Netherlands

Received 16 December 2002
*Kvantovaya Elektronika* **33** (10) 856 – 860 (2003)
Translated by M.N. Sapozhnikov

The output power of RF-discharge-pumped slab CO lasers cooled down to cryogenic temperatures achieves $\sim 1$ kW at a lasing efficiency of 25 % [3].

We developed earlier the one-dimensional model of the RF discharge for a slab $CO_2$ laser [4]. This model was used [5] to calculate the volt – power characteristics of the RF discharge in mixtures containing CO. A comparison between the calculated and measured [6] volt – power characteristics of the RF discharge showed their good agreement. The RF discharge model was supplemented in Ref. [5] by a block for calculating the vibrational kinetics of CO molecules, which made it possible to calculate the small-signal gain spectrum in a RF-discharge-pumped slab CO laser.

The aim of this paper is the further development of the one-dimensional model of a RF-discharge-pumped slab laser taking into account stimulated emission, which allows us to find the spectral and power parameters of the laser.

## 2. Theoretical model

We assume that the discharge is homogeneous along the electrodes, so that it is sufficient to find the spatial profiles of the quantities over the interelectrode distance. The model takes one type of positive ions into account. The concentration of negative ions was neglected because of a rapid destruction of the $O^-$ ions in collisions with the CO molecules. The continuity equation for positive ions was solved together with the continuity equation for the electron concentration and the Poisson equation for an electric field. The gas temperature was determined from the stationary heat conduction equation, in which the energy extraction by laser radiation was taken into account. Because the laser power was unknown at the beginning of calculations, the entire calculations were performed through a number of iterations. At the first step, we assumed that the total power of the discharge converts to heat. The heat conductivity of the gas mixture was calculated from the heat conductivities of individual components using the procedure described in Ref. [7]. The heat conductivities of individual components and their temperature dependences were taken from handbook [8].

The average electron energy $\bar{\varepsilon}$ was calculated by solving the nonstationary equation for $\bar{\varepsilon}$ taking into account the electron heat conductivity. The energy $\bar{\varepsilon}$ was calculated at each instant of time at all the points of the interelectrode gap and was used for calculating ionisation constants, which were found preliminary as the functions of $\bar{\varepsilon}$ by the numerical solution of the Boltzmann equation for the energy distribution function for electrons. The transfer coefficients

were also tabulated and used for solving the nonstationary equation for the average electron energy and the continuity equation.

We used earlier a similar model to simulate the RF discharge in the He–Ar–Xe mixture [9]. The equations were supplemented with the corresponding boundary and initial conditions. The voltage across the discharge gap was found from the specified power of the RF field. We used in numerical calculations a mesh with a spatial step decreasing toward electrodes. The typical number of spatial steps used in calculations was about of 100. To obtain the stationary solution, a few thousands of the cycles of the RF field should be calculated. The model of the RF discharge and the numerical algorithm are described in more detail in paper [4].

The fraction of power spent for excitation of the vibrational levels of CO molecules was calculated from the obtained distributions of the reduced electric field strength $E/N$ (where $N$ is the density of neutral particles) and the power density in the discharge. The fraction of the electron energy spent to excite the vibrational levels was found from the stationary Boltzmann equation for the unexcited gas as a function of $E/N$. Because the characteristic times of the vibrational kinetics under our conditions are much longer than the period of the exciting electric field, the populations of the vibrational levels are determined by the period-averaged power spent for their excitation.

The spatial distributions of the translational temperature of the gas and the period-averaged power spent for excitation of the vibrational levels were used in calculations of the stationary local vibrational distribution functions (VDFs) of CO molecules at different points of the interelectrode gap. Our estimates show that the diffusion of vibrationally excited molecules can be neglected. The VDFs were found by solving the stationary equations of the vibrational kinetics of CO molecules by the iteration method described in Ref. [10]. The VV-exchange and VT-relaxation constants, and the Einstein coefficients for individual transitions and collision broadening of a line were taken from Ref. [10].

The lasing power spectrum was calculated assuming that the field intensity distribution $I_0(x)$ at the chosen vibrational–rotational transition $v, j-1 \rightarrow v-1, j$ is a specified function of the coordinate $x$. The specific form of the function $I_0(x)$ is determined by the mode composition of radiation. The equations of the vibrational kinetics contain the terms of the type $[I_v/(hv_v)]I_0(x)g_{vj}(x)$, where $I_v/(hv_v)$ is the total intensity of radiation at the given transition; $v_0$ is the radiation frequency; and $g_{vj}(x)$ is the gain at this transition. The value of $I_v/(hv_v)$ was found from the condition of the equality of the gain averaged over the interelectrode gap to the resonator losses $\Gamma$:

$$G_j = \int_0^d I_0(x)g_j(x)\mathrm{d}x \Big/ \int_0^d I_0(x)\mathrm{d}x = \Gamma, \qquad (1)$$

where $d$ is the interelectrode distance. In the slab geometry, a one-dimensional unstable resonator is commonly used. In this case, $\Gamma = \ln M/(2L)$, where $M$ is the magnification of the resonator and $L$ is the length of the amplifying medium.

The emission spectrum of the free-running laser was found by calculating the coefficients $I_v/(hv_v)$ beginning from the lower level $v$, for which the averaged small-signal gain $G_{vj}^0$ exceeded the resonator losses. In this case, the number of the rotational transition was found from the condition of maximum of $G_{vj}^0$ over all $j$. The procedure was terminated for the transitions with the maximum small-signal gain averaged over $j$, equal to the resonator losses.

Although the intensity of higher-lying transitions weakly affects the intensity of lower-lying transitions, our computational program makes provision for further iterations to improve the accuracy of calculation of the free-running laser spectrum. For typical conditions, the maximum relative difference of the average gain for all $v$ at which lasing occurs from the resonator losses was 12 % after the first iteration and 2.5 % after the second iteration. The efficiency of the laser was found from the total output power. Then, the RF discharge was calculated again taking into account the energy extraction by laser radiation. This procedure was continued until the required accuracy of the calculation of the laser efficiency was achieved.

## 3. Results and discussion

We performed numerical simulations for the conditions corresponding to the experiments [3] with the gas mixture $CO : He : Xe : O_2 = 24 : 71 : 4 : 1$ at a pressure of 60 Torr. The frequency of the exciting field was 90 MHz, the interelectrode distance was 0.2 cm, and the specific excitation power was 23 W cm$^{-3}$. The walls were cooled down to cryogenic temperatures in experiments. Because no exact data on the wall temperature $T_w$ were reported in Ref. [3], we performed simulations for $T_w = 80 - 130$ K.

We used in simulations two distributions of the output intensity over the laser aperture: $I_0(x) \sim 1/d$, which approximately corresponds to multimode lasing, and $I_0(x) \sim (2/d) \times \sin^2(\pi x/d)$, which corresponds to lasing on the fundamental waveguide mode. Under real experimental conditions, the gas is heated, resulting in defocusing, and the mode structure changes. The intensity distribution of the modes in a slab laser on the IR transitions of Xe was studied taking into account defocusing in Ref. [11]. In this paper, we did not study the mode composition of radiation and for this reason analysed the two model cases.

The total specific pump power near the walls is low and is determined by the heating of ions [curve (*1*) in Fig. 1]. The excitation power of the vibrational levels of the CO molecule increases with distance from the wall [curve (*2*)]. The translational temperature of the gas near the walls is still low, and the power of laser radiation emitted by the unit volume increases with distance from the wall [curves (*3*), (*3′*)]. In the case of lasing at the fundamental mode [curve (*3′*)], a low radiation intensity near the wall cannot provide the extraction of energy from the vibrational levels. The energy-extraction efficiency noticeably decreases at the centre of the discharge due to an increase in the translational temperature, while the VT relaxation increases [curve (*4*)]. The energy losses due to the VV exchange and spontaneous emission are small and are 6 % and 1.6 %, respectively, at the discharge centre.

Analysis of the simulation results showed that the distribution of the gas temperature in the discharge gap is close to a parabolic one. Table 1 presents the translational gas temperatures at the discharge centre for different wall temperatures in the absence of lasing, during multimode lasing, and lasing at the fundamental mode. One can see that

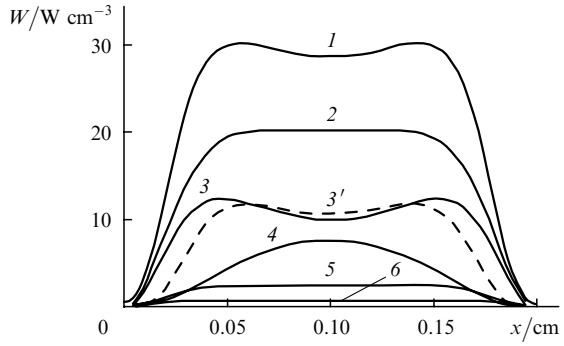


**Figure 1.** Distributions of different power densities along the discharge gap: (*1*) total power deposited to the discharge; (*2*) power exciting the vibrational levels of the CO molecules; (*3*, *3′*) output power; power released due to (*4*) VT relaxation and (*5*) VV exchange; and the spontaneous emission power density (*6*) upon multimode lasing (*1–6*) and lasing at the fundamental mode (*3′*); $T_w = 100$ K.

**Table 1.** Translation gas temperature $T$ at the centre of the discharge gap at different wall temperatures $T_w$.

| $T_w$/K | $T$/K | | |
|---|---|---|---|
| | No lasing | Multimode lasing | Lasing on the fundamental mode |
| 80 | 311 | 224 | 240 |
| 100 | 322 | 255 | 264 |
| 120 | 333 | 299 | 325 |
| 130 | 338 | 322 | – |

laser emission at high lasing efficiencies noticeably reduces the temperature at the discharge centre.

Figure 2 shows the VDFs for CO molecules at different points of the discharge gap in the absence of lasing and in the case of multimode lasing. The vibrational temperature of the lower levels of the CO molecule increases from the wall to the discharge centre due to the increase in the translational temperature of the gas and the excitation power of vibrational levels. When lasing begins, the population decreases only on the levels whose numbers are higher than the number corresponding to the lower boundary of the region involved in lasing.

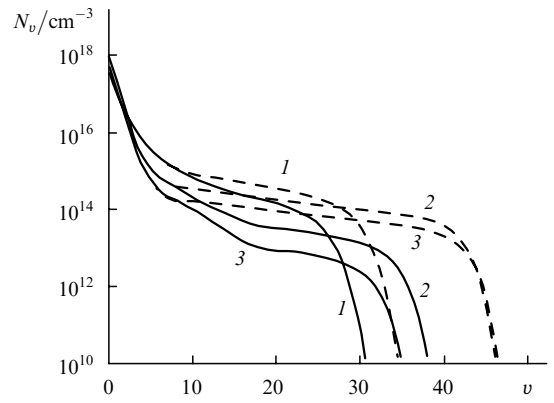


**Figure 2.** VDFs of CO molecules for $x = 0.1$ (*1*), 0.013 (*2*), and 0.008 cm (*3*) in the case of multimode lasing (solid curves) and in the absence of lasing (dashed curves); $T_w = 100$ K.

The decrease in excitation of the vibrational levels near the walls and a substantial increase in the translational gas temperature at the discharge gap centre leads to a noticeable change in the gain at different vibrational–rotational transitions along the discharge gap. Figure 3 shows the distributions of the small-signal gain $g^0_{vj}$ over the interelectrode gap for the $9P(15)$, $10P(13)$, $11P(12)$, $12P(11)$, and $13P(11)$ transitions (here, notation $vP(j)$ means the $v, j-1 \to v-1, j$ transition). The numbers of vibrational transitions are taken from the condition of exceeding of space-averaged small-signall gain over the resonator losses: $G^0_{vj} > \Gamma$. The numbers of rotational transitions correspond to the maximum gain $G^0_{vj}$ over all $j$ for the given $v$.

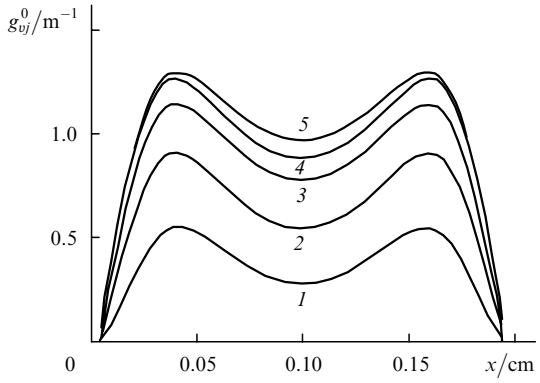


**Figure 3.** Distributions of the small-signal gain $g^0_{vj}$ over the interelectrode gap for the vibrational–rotational transitions $9P(15)$ (*1*), $10P(13)$ (*2*), $11P(12)$ (*3*), $12P(11)$ (*4*), and $13P(11)$ (*5*) for $T_w = 100$ K.

The development of lasing results in the saturation of the gains. Figure 4 shows the distributions of the gains $g_{vj}$ for multimode lasing. The transitions are the same as in Fig. 3. The gain for the specified intensity $I_{vj}$ can be recalculated from the small-signal gain $g^0_{vj}$ and the saturation intensity $I^s_{vj}$ using a simple expression $g_{vj} = g^0_{vj}/(1 + I_{vj}/I^s_{vj})$. By using this expression for the discharge gap centre and taking the values of $g_{vj}$, $g^0_{vj}$, and $I_{vj}$ from the numerical calculation, we obtain for the conditions in Fig. 4 that $I^s_{vj} = 1030$, 660, 430, 280, and 84 W cm$^{-2}$ for the $9P(15)$, $10P(13)$, $11P(12)$, $12P(11)$, and $13P(11)$ transitions, respectively. This means that the saturation intensity in the CO laser is determined not only by the rate constants of elementary processes but also by the

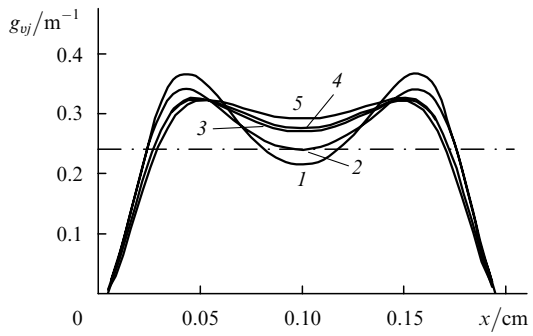


**Figure 4.** Distributions of the gain $g_{vj}$ over the interelectrode gap for the vibrational–rotational transitions $9P(15)$ (*1*), 10P(13) (*2*), $11P(12)$ (*3*), $12P(11)$ (*4*), and $13P(11)$ (*5*) in the case of multimode lasing for $T_w = 100$ K. The dash-dotted straight line is resonator losses.

excitation level of the active medium, as was mentioned earlier in paper [12].

The CO laser emits simultaneously at many vibrational–rotational transitions. We study in our model the lasing at many vibrational transitions, but for each vibrational transition in the stationary regime, lasing is considered at the rotational transition corresponding to the maximum gain $G_v$ for all $j$ averaged over the discharge gap. Figure 5 shows the maximum small-signal gain $G_v^0$ for all $j$ and the given $v$ averaged over the discharge gap, as well as the gain $G_v$ for multimode lasing as functions of $v$. In the case of lasing, the numbers of rotational transitions corresponding to the maximum gain are displaced to the larger values of $j$, which is caused by the decrease in the population of vibrational levels (see Fig. 2).

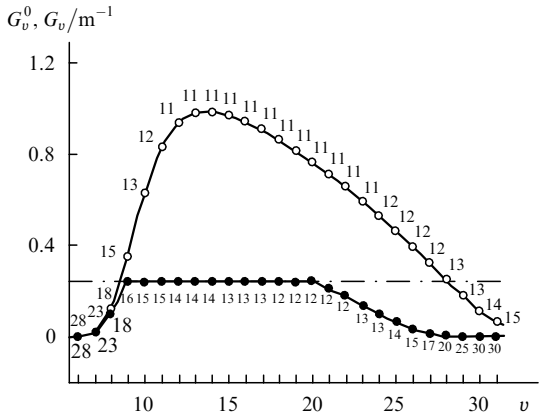


**Figure 5.** Averaged small-signal gain $G_v^0$ maximal over $j$ (open circles) and the averaged gain $G_v$ maximal over $j$ in the case of multimode lasing (dark circles) for $T_w = 100$ K. The numbers at points are the values of $j$ for which the gain is maximal. The dash-dotted straight line is resonator losses.

The change in the spectrum of the specific output power with increasing the wall temperature $T_w$ from 80 to 120 K is shown in Fig. 6. For $T_w = 120$ K, the lower edge of the lasing spectrum is displaced by one vibrational transition to the larger values of $v$, and the numbers of rotational transitions also are displaced by one–two units to the larger values of $j$ compared to $T_w = 80$ K. In the case of lasing at the fundamental mode, the laser radiation is concentrated in the central region of the discharge, where the translational temperature of the gas is higher. This leads to the increase in $j$ (cf. Figs 6b and d).

The dependence of the lasing efficiency on the wall temperature $T_w$ is shown in Fig. 7 [curve (*2*)]. The lasing efficiency decreases with increasing $T_w$ almost linearly. Such behaviour is qualitatively consistent with experimental data [13, 14]. To illustrate the role of the energy extraction during gas heating, Fig. 7 shows the lasing efficiency determined at the first step, when we assumed that the entire power converts to heat [curve (*1*)]. One can see that the lasing efficiency, calculated neglecting the energy extraction by laser radiation, is substantially lower than the real efficiency. During lasing at the fundamental mode, the field is concentrated at the centre of the discharge gap, where the translational temperature of the gas is higher, resulting in the reduction of the lasing efficiency [curve (*3*)]. A similar decrease in the lasing efficiency on passing to the single-mode regime was observed in paper [14]. The authors of Ref. [3] obtained experimentally the lasing efficiency upon cryogenic cooling equal to 25 %. Our calculations (for multimode lasing) show that such efficiency is obtained at $T_w = 115$ K (Fig. 7). Although the wall temperature was

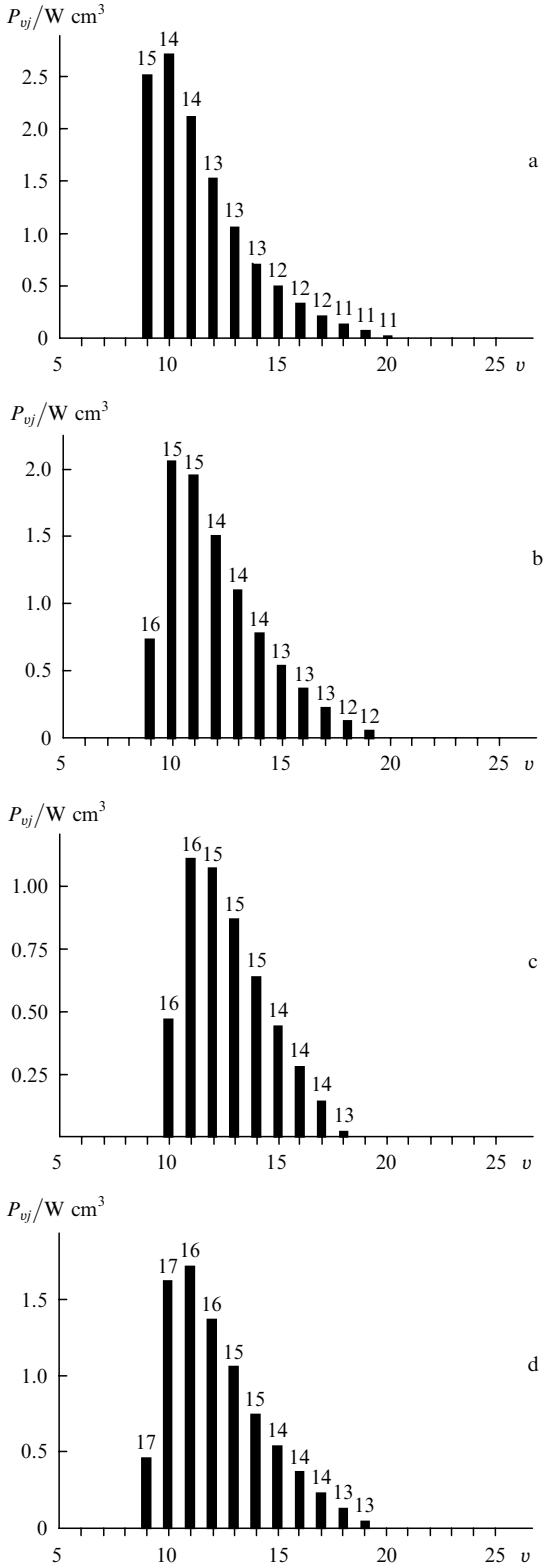


**Figure 6.** Spectra of multimode lasing (a–c) and lasing on the fundamental mode (d) for $T_w = 80$ (a), 100 (b, d), and 120 K (c). The numbers at bars are the values of $j$.

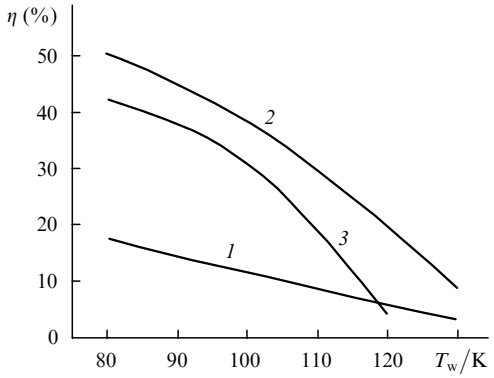


**Figure 7.** Dependences of the lasing efficiency $\eta$ on the wall temperature $T_w$ in the absence of a decrease in heating due to lasing (*1*), for multimode lasing (*2*) and lasing on the fundamental mode (*3*).

not measured in Ref. [3], the value 115 K seems to be quite probable for these experiments.

The lasing efficiency $\eta$ is determined by the product $\eta = \eta_v \eta_{pr}$ of the efficiency $\eta_v$ of conversion of the energy deposited to the discharge to the vibrational energy by the efficiency $\eta_{pr}$ of conversion of the vibrational energy to laser radiation. The dependences of $\eta_v$ and $\eta_{pr}$ on the wall temperature $T_w$ are shown in Fig. 8. A variation in $T_w$ weakly affects the efficiency $\eta_v$, but noticeably reduces $\eta_{pr}$ due to the decrease in the gain on vibrational–rotational transitions. The passage from multimode lasing to lasing on the fundamental mode weakly affects $\eta_v$, but reduces $\eta_{pr}$ [cf. curves (*2*)] because during lasing at the fundamental mode the field is localised at the centre of the discharge gap, where the temperature is higher.

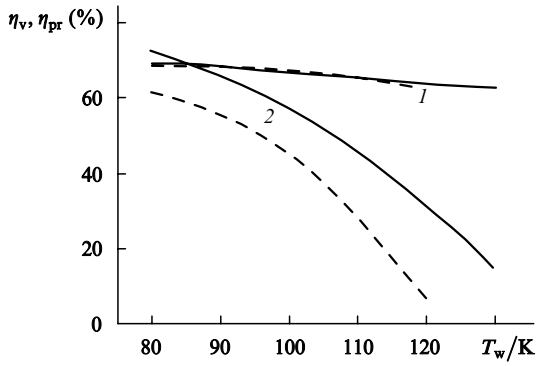


**Figure 8.** Discharge efficiency $\eta_v$ (*1*) and the efficiency $\eta_{pr}$ of conversion of the vibrational energy to laser radiation (*2*) as functions of the wall temperature for multimode lasing (solid curves) and lasing on the fundamental mode (dashed curves).

## 4. Conclusions

We have developed the one-dimensional model of an RF-discharge-pumped slab CO laser. The model allows one to calculate the spatial structure of a capacitive RF discharge corresponding to the distribution of the translational temperature of the gas determined taking into account the energy extraction by laser radiation. By specifying the profile of laser radiation intensity over the interelectrode gap, we have found the energy and spectral characteristics of the CO laser in the stationary regime. The effect of the wall temperature and the mode composition of radiation on the output power and spectrum of the laser have been studied theoretically. The model predicts a substantial influence of lasing on the gas temperature and discharge characteristics. The results of our simulations are in reasonable agreement with the lasing efficiency measured in paper [3].

***Acknowledgements.*** The authors thank A.A. Ionin for useful discussions of the statement of the problem. This work was partially supported by the Russian Foundation for Basic Research (Grant No. 01-02-17136) and the ISTC (Grant No. 2415P).

## References

1. Colley A.D., Villarreal F., Cameron A.A., Vitruk P.P., Baker H.J., Hall D.R. *NATO ASI Ser. 3: High Technology*, **10**, 89 (1995).
2. Udalov Y.B., Tskhai S.N., Peters P.J.M., Witteman W.J., Kochetov I.V., Ochkin V.N. *NATO ASI Ser. 3: High Technology*, **10**, 73 (1995).
3. Xin Jianguo, Zhang Wang, Jiao Wentao. *Appl. Phys. Lett.*, **75**, 1369 (1999).
4. Starostin S.A., Boller K.J., Peters P.J.M., Udalov Yu.B., Kochetov I.V., Napartovich A.P. *Fiz. Plasmy*, **28**, 68 (2002) [*Plasma Physics Reports*, **28**, 63 (2002)].
5. Ionin A.A., Klimachev Yu.M., Kochetov I.V., Napartovich A.P., Sinitsyn D.V., Starostin S.A., Terekhov Yu.V. Preprint FIAN (53) (Moscow, 2001).
6. Kunn V.V., Leont'ev V.G., Novgorodov M.Z., Ochkin V.N., Shishkanov E.P., Stepanov V.A. *Proc. XXII ICPIG* (Haboken, 1995) Vol. 3, p. 67.
7. Wahid Syed M.S., Madhusudana C.V. *Intern. J. Heat Mass Transfer*, **43**, 4483 (2000).
8. Grigor'ev I.S., Meilikhov E.Z. (Eds) *Fizicheskie velichiny. Spravochnik* (Handbook of Physical Quantities) (Moscow: Energoatomizdat, 1991).
9. Starostin S.A., Peters P.J.M., Van der Pool G., et al. *Fiz. Plazmy*, **27**, 458 (2001) [*Plasma Physics Reports*, **27**, 432 (2001)].
10. Konev Yu.B., Kochetov I.V., Pevgov V.G., Sharkov V.F. Preprint IAE-2821 (Moscow, 1997).
11. Blok F.J., Elkin N.N., Kochetov I.V., Napartovich A.P., Peters P.J.M., Starostin S.A., Troshchieva V.N., Udalov Y.B., Witteman W.J. *IEEE J. Quantum Electron.*, **35**, 1786 (1999).
12. Napartovich A.P., Novobrantsev I.V., Starostin A.N. *Kvantovaya Elektron.*, **4**, 2125 (1977) [*Sov. J. Quantum Electron.*, **7**, 1216 (1977)].
13. Zhao H., Baker H.J., Hall D.R. *Appl. Phys. Lett.*, **59**, 281 (1991).
14. Colley A.D., Villarreal F., Baker H.J., Hall D.R. *Appl. Phys. Lett.*, **64**, 2914 (1994).